

Power Factor Estimation of Distributed Energy Resources Using Voltage Magnitude Measurements

Samuel Talkington, Santiago Grijalva, and Matthew J. Reno

Abstract—This paper presents a new method for the estimation of the injection state and power factor of distributed energy resources (DERs) using voltage magnitude measurements only. A physics-based linear model is used to develop estimation heuristics for net injections of real and reactive power at a set of buses under study, allowing a distribution engineer to form a robust estimate for the operating state and the power factor of the DER at those buses. The method demonstrates and exploits a mathematical distinction between the voltage sensitivity signatures of real and reactive power injections for a fixed power system model. Case studies on various test feeders for a model of the distribution circuit and statistical analyses are presented to demonstrate the validity of the estimation method. The results of this paper can be used to improve the limited information about inverter parameters and operating state during renewable planning, which helps mitigate the uncertainty inherent in their integration.

Index Terms—Decentralized power system control, detection and estimation, power factor, sparse approximation.

I. INTRODUCTION

THE success of the ongoing global energy transition is contingent upon the development of accurate models of distributed energy resources (DERs) to be used for the planning and operation of power systems. The rapid deployment of these DERs consequently leads to the cases of limited data availability and uncertainty regarding unobservable im-

pacts to the distribution system.

One of the remaining limiting factors for high penetrations of DERs is the risk of unforeseen violations of engineering constraints due to unacceptable voltage rises from volatile power injections inherent in DERs. Direct curtailment is typically one of the solutions to this issue. However, this is unfavorable due to the loss of clean generation and revenue for the DER owner.

Advanced inverter technologies have emerged as central elements of the solution to these issues, and research works on their impact on distribution networks have appeared swiftly in [1]–[4]. Additionally, the IEEE 1547-2018 standard updates now require all inverters to have reactive power and voltage regulation capabilities [5]. However, utilities and independent system operators (ISOs) may have limited information about these inverters, and therefore may be unable to accurately predict their effects on a distribution network. Frequently, these organizations may only have access to voltage measurements from metering devices and may have limited information about the overall operating conditions of inverter-based resources, including the power factor, curtailment, and voltage control parameters of the system. If utilities have access to this information, it may be incorrect or out-of-date due to the changes over time [6]. The inverters used in grid-connected photovoltaic (PV) systems have the capability to curtail active power output as well as inject and absorb reactive power, according to the behavior defined by a control curve. Frequently, non-unity power factor control settings are applied to inverter installations to reduce voltage problems that may be caused by the DER.

The primary contributions of this paper are the solutions to the inverse problem of estimating an unknown fixed power factor control setting for a DER. The methods presented here have remarkably low data input requirements, in that only voltage magnitude measurements are required. Although the deployment of advanced metering infrastructure (AMI) continues to expand, most utilities only have access to net energy measurements and do not have access to reactive power measurements, making the calculation of a DER power factor setting impossible. Through the methods developed in this paper, we show that it is possible to recover this setting with highly incomplete measurement data. This is achieved through a physics-based linearization of the AC power flow manifold, through which we demonstrate a novel result that the voltage magnitude sensitivities to real and reactive power injections are linearly independent for a fixed

Manuscript received: January 31, 2021; accepted: June 16, 2021. Date of CrossCheck: June 16, 2021. Date of online publication: July 31, 2021.

This material is based upon the work supported by the U.S. Department of Energy's Office of Energy Efficiency and Renewable Energy (EERE) under Solar Energy Technologies Office (SETO) Agreement Number 34226. Sandia National Laboratories is a multi-mission laboratory managed and operated by National Technology and Engineering Solutions of Sandia, LLC, a wholly owned subsidiary of Honeywell International, Inc., for the U.S. Department of Energy's National Nuclear Security Administration under contract DENA0003525. This paper describes objective technical results and analysis. Any subjective views or opinions that might be expressed in the paper do not necessarily represent the views of the U.S. Department of Energy or the United States Government. The authors would like to thank Logan Blakely for his insightful input and comments during the early stages of the project. The authors would also like to thank Dr. Matthieu Bloch for an insightful conversation on hyperparameter tuning.

This article is distributed under the terms of the Creative Commons Attribution 4.0 International License (<http://creativecommons.org/licenses/by/4.0/>).

S. Talkington (corresponding author) and S. Grijalva are with the School of Electrical and Computer Engineering, Georgia Institute of Technology, Atlanta, GA 30318, USA (e-mail: talkington@gatech.edu; sgrijalva@ece.gatech.edu).

M. J. Reno is with the Electric Power Systems Research Department, Sandia National Laboratories, Albuquerque, NM 87123, USA (e-mail: mjreno@sandia.gov).

DOI: 10.35833/MPCE.2021.000086



distribution network model. The result allows for a simultaneous estimation of the real and reactive power injection states at a set of DER interconnection points under study, which is used to construct a robust estimate for the power factor.

Furthermore, we enhance the predictive power and applicability of the method by deriving both a regularized regression model and a sparse approximation model, recasting the estimation as convex optimization problems. These reformulations improve the robustness of the estimation method in cases of a poor or inaccurate distribution system model or user uncertainty of the DER's location, respectively.

II. BACKGROUND

The theorem in [7] proves that for a fixed power network with \mathcal{S} slack buses, \mathcal{N} PQ buses, and nodal admittance matrix \mathbf{Y} , the complex voltage sensitivity coefficients at each bus $i \in \mathcal{N}$ to real and reactive power injections P_l, Q_l at each bus $l \in \mathcal{N}$ are unique solutions to the following two systems of differential equations:

$$1\{i=l\} = \frac{\partial \bar{V}_i}{\partial P_l} \sum_{j \in \mathcal{S} \cup \mathcal{N}} Y_{i,j} \bar{V}_j^* + \bar{V}_i \sum_{j \in \mathcal{N}} Y_{i,j} \frac{\partial \bar{V}_j^*}{\partial P_l} \quad (1)$$

$$-j1\{i=l\} = \frac{\partial \bar{V}_i}{\partial Q_l} \sum_{j \in \mathcal{S} \cup \mathcal{N}} Y_{i,j} \bar{V}_j^* + \bar{V}_i \sum_{j \in \mathcal{N}} Y_{i,j}^* \frac{\partial \bar{V}_j^*}{\partial Q_l} \quad (2)$$

where \bar{V}_i and \bar{V}_j are the complex nodal voltages; and \bar{V}_i^* and \bar{V}_j^* are the complex conjugate nodal voltages.

These equations and the research work in [7] use complex voltage values, but this information is not available for a distribution system without access to phasor measurement unit (PMU) data. Our work exploits the use of voltage magnitude sensitivities without angle measurements, which are more common in realistic sensor data.

Researchers have taken the interest in data-driven modeling of advanced inverters, but little work has been done in terms of the estimation of their operational parameters and behaviors. Reference [2] develops both linear and nonlinear state estimators for voltage magnitudes of the point of common coupling (PCC) using a Kalman filter. Intermittent measurements and packet loss are considered as a source of measurement error, but their linear model relies on complete knowledge of the power flow Jacobian, generation, and load profiles. In practice, the availability of such data may be challenging. Reference [8] attempts a similar problem using limited load and PV profile data to form representative scenarios [8].

Research works such as in [4] use a variation of the optimal power flow to estimate optimal control settings for advanced inverters, while [9] and [10] develop a decentralized control approach to estimate optimal smart inverter settings based on volt-var, volt-watt, or power factor control. The feeder is analyzed using time-series simulation and various inverter control parameters, ranking their optimality based on the number of violations of voltage constraints.

An interest has grown in analyzing how distributed inverter-based systems behave with fixed control parameters [1], [11], [12]. Reference [1] presents a fast quasi-static time-se-

ries algorithm for computing the impacts of dynamic var control, providing an estimate for the states of all controllers with a candidate control curve. In [12], a robust estimate for solar PV energy curtailment is provided for a distributed generation system operating with a fixed volt-watt curve.

The literature has only recently explored inverse problems in this domain. Approaches such as those in [13], [14] use voltage sensitivities as training data to detect the presence of a solar PV installation on a distribution system using voltage sensitivities. Additional methods for the detection of PV locations and size, and the estimation of the overall distribution hosting capacity of system are developed using a Monte Carlo approach in [15].

However, the literature lacks the exploration into the inverse problems of estimating DER settings and operational parameters such as the power factor using data-driven methods.

III. METHODOLOGY

Throughout this paper, we consider a distribution network with \mathcal{M} nodes and \mathcal{L} possible points of interconnection for a DER system, where $\mathcal{L} \subset \mathcal{M}$.

A. Definitions

1) Voltage Magnitude Sensitivities

The sensitivity matrix of node voltages to both real and reactive power injections is well understood [7], [13]. These entries of the matrix are typically defined as the changes in voltage at bus i with respect to a real or reactive power injection at bus l . In this paper, voltage sensitivities refer to changes in voltage magnitude since distribution sensors do not provide voltage angle measurements without highly time-synchronized data like PMUs.

Assuming circuit parameters are fixed and injection magnitudes are normalized, the voltage sensitivities to real and reactive power injections, while linearly related, are intrinsically different functions. This distinction has been noted [7] and is illustrated here as an example.

We define the voltage sensitivity matrix of a circuit as the change in voltage magnitude at any node $i \in \mathcal{M}$ due to the presence of a real or reactive power injection at another "candidate" injection bus $l \in \mathcal{L}$. The formulation we will use in this paper alternates the columns between real and reactive injections, as shown in (3).

$$\mathbf{S}^{PO} \triangleq \frac{\partial V_i}{\partial [P_l, Q_l]} \quad \forall i \in [1, \mathcal{M}], \forall l \in [1, \mathcal{L}] \quad (3)$$

where V_i is the voltage magnitude measurement. This gives us an $\mathcal{M} \times (2\mathcal{L})$ sensitivity matrix that appears as follows:

$$\mathbf{S}^{PO} \triangleq \begin{bmatrix} \frac{\partial V_i}{\partial P_l} & \frac{\partial V_i}{\partial Q_l} & \cdots & \frac{\partial V_i}{\partial P_{\mathcal{L}}} & \frac{\partial V_i}{\partial Q_{\mathcal{L}}} \\ \vdots & \vdots & & \vdots & \vdots \\ \frac{\partial V_N}{\partial P_l} & \frac{\partial V_N}{\partial Q_l} & \cdots & \frac{\partial V_N}{\partial P_{\mathcal{L}}} & \frac{\partial V_N}{\partial Q_{\mathcal{L}}} \end{bmatrix} \in \mathbb{R}^{\mathcal{M} \times (2\mathcal{L})} \quad (4)$$

This matrix effectively captures two linearly independent signatures of the power system and describes the response of

the node voltages to real and reactive power injections.

In practice, these matrices can be formed using perturb and observe methods [7], [13], [14], our method is described in Algorithm 1 in the subsequent section.

We will denote each column of the interleaved \mathbf{S}^{PQ} matrix as \mathbf{s}_l , where $l=1, 2, \dots, 2\mathcal{L}$. Note that this matrix has full column rank when formulated using a power system model without any voltage regulation equipment, and that pairs of columns for electrically identical buses such as those connected by switches or fuses are excluded. This verifies that the columns are linearly independent, and implies that the signatures of voltage sensitivities to real and reactive power are inherently different from the perspective of signal processing.

This distinction can also be motivated through a graphical example using simulated results from the IEEE 13-bus test feeder. If the submatrices of the \mathbf{S}^{PQ} matrix associated with real and reactive power injections are compared graphically, the functions have highly different behaviors. Submatrices of \mathbf{S}^{PQ} containing the alternating sensitivity columns corresponding to real or reactive power is shown in Fig. 1. Each matrix column \mathbf{s}_l captures the normalized changes in V_i to a real or reactive power injection on bus l of the IEEE 13-bus test feeder. The intrinsic difference in the signatures of the system response for different injection types becomes apparent. For simplicity, the suffix(i) to denote phase i of each bus for the remainder of this paper, where $i=1, 2, 3$ represents phases A, B, and C, respectively.

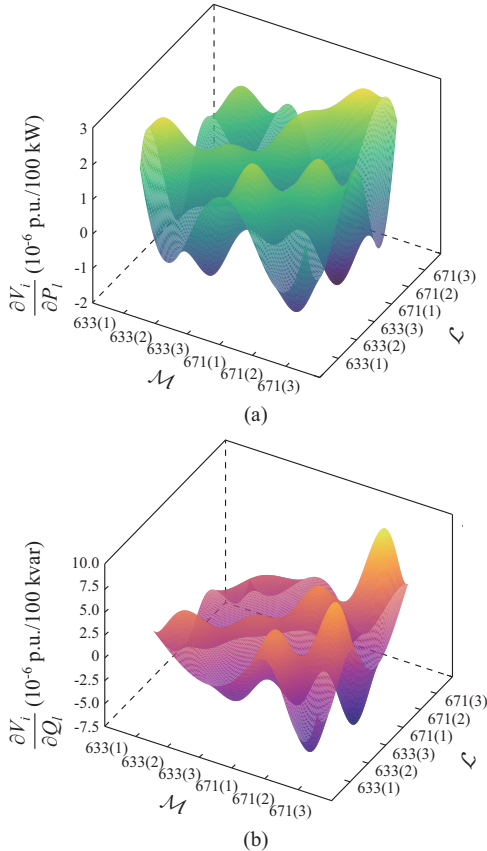


Fig. 1. Submatrices of \mathbf{S}^{PQ} containing alternating sensitivity columns corresponding to real or reactive power. (a) Sensitivity of node voltage to real power. (b) Sensitivity of node voltage to reactive power.

The real and reactive power injection columns of \mathbf{S}^{PQ} , while linearly independent, may still exhibit some multicollinearity. We will later show how this contributes to the variance of the least-squares estimator in some use cases.

2) Measurement Data

When working with time-series data, we assume that networked voltage meters will give the user access to voltage profile data $v_i(t)$ at bus i for \mathcal{M} nodes across time horizon T . By taking the simple difference between the voltage samples across time, we can form a difference matrix $\mathbf{D}' \in \mathbb{R}^{\mathcal{M} \times (T-1)}$ as follows:

$$\mathbf{D}' \triangleq (\Delta v_{i,\tau}) \quad \forall t \in [1, T-1], i \in [1, \mathcal{M}] \quad (5)$$

$$\Delta v_{i,\tau} = v_i(t) - v_i(t-1) \quad (6)$$

where $\Delta v_{i,\tau}$ is the voltage deviation.

Furthermore, we define a measurement vector $\bar{\mathbf{d}} \in \mathbb{R}^{\mathcal{M}}$ as a column vector containing samples of each row of the difference matrix at a specific time differential point of interest τ^* :

$$\bar{\mathbf{d}} \triangleq (\Delta v_{i,\tau^*}) \quad \forall i \in [1, \mathcal{M}] \quad (7)$$

$$\Delta v_{i,\tau^*} = v_i(\tau^*) - v_i(\tau^* - 1) \quad (8)$$

When considering solar PV, time intervals with low irradiance such as nighttime or cloudy days will have near-zero changes in voltage due to the real and reactive power injections of the PV and its corresponding inverter. Thus, it can be challenging to select τ^* in practice for each bus i .

One choice is to simply select τ^* during midday, during which the irradiance, power magnitude as well as the variance of the injection between t^* and $t^* - 1$ are likely to be the highest [13], [14]. This behavior is shown in Fig. 2. A 12-hour, 15-min granularity solution yields a total time horizon of $T = 287$. Voltage deviations due to volatile real or reactive power injections from the system are more likely to occur during midday and are near-zero during the time of low irradiance.

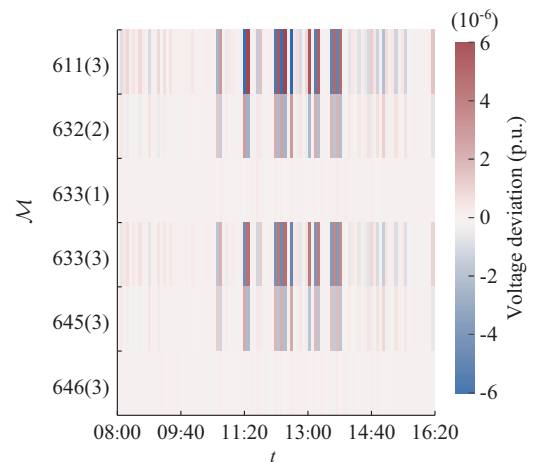


Fig. 2. A subset of voltage deviation entries in $\mathbf{D}' \in \mathbb{R}^{\mathcal{M} \times (T-1)}$ from 08:00 to 16:20 for 100 kW solar PV installation with power factor of 0.8 on 633(1) of the IEEE 13-bus feeder.

Generally, the measurement vector $\bar{\mathbf{d}}$ is most likely to best

approximate a linear combination of columns of \mathbf{S}^{PQ} during times of maximum variance in the voltage profile between time points. $\bar{\mathbf{d}}$ captures the change in voltage magnitude during the time differential τ^* due to a PV injection change at a location l . When the vector $\bar{\mathbf{d}}$ is normalized by the size of the PV system, the contributions of the columns of \mathbf{S}^{PQ} corresponding to real and reactive power injections from a PV and var-dispatching inverter located at bus l can be estimated with linear regression models.

Since sensor data noise will primarily be driven by additive white Gaussian noise (AWGN), we assume that all model errors are distributed according to a standard normal $\epsilon \sim \mathcal{N}(0, \sigma_\epsilon^2)$.

B. Estimation Methodology

1) Least-squares Regression

The measurements obtained from the sensors will contain noise due to manufacturing errors, sensor class, or model inaccuracies. Hence, when projecting the $\bar{\mathbf{d}}$ vector on the subspace of \mathbf{S}^{PQ} , we obtain close but not exactly equal injection contributions. Using the measurement vector $\bar{\mathbf{d}}$ and the voltage sensitivity matrix \mathbf{S}^{PQ} , we can form a multiple linear regression approximation to estimate the corresponding injection type, location, and quantity as:

$$\bar{\mathbf{d}} \approx x_0 \frac{\partial V}{\partial P_l} + x_1 \frac{\partial V}{\partial Q_l} + \dots + x_{2\mathcal{L}-1} \frac{\partial V}{\partial P_{\mathcal{L}}} + x_{2\mathcal{L}} \frac{\partial V}{\partial Q_{\mathcal{L}}} + \epsilon \quad (9)$$

With many parameter estimation problems, we are estimating a vector $\hat{\mathbf{x}}$ when we multiply by our design matrix. We yield an approximation of the measurement targets as:

$$\hat{\mathbf{d}} = \mathbf{S}^{PQ} \hat{\mathbf{x}} \quad (10)$$

where $\hat{\mathbf{x}}$ is the coefficient vector that results in the minimization of the sum of squared errors [16]. These problems are known to have a unique least-squares solution as shown in (11). Later, we will denote the least-squares solution as $\hat{\mathbf{x}}_{lsq}$ to differentiate the solution from the other methods that we will discuss.

$$\begin{cases} \min_{\mathbf{x} \in \mathbb{R}^{2\mathcal{L}}} \|\bar{\mathbf{d}} - \mathbf{S}^{PQ} \mathbf{x}\|_2^2 \\ \hat{\mathbf{x}} = ((\mathbf{S}^{PQ})^T \mathbf{S}^{PQ})^{-1} (\mathbf{S}^{PQ})^T \bar{\mathbf{d}} \end{cases} \quad (11)$$

2) Shrinkage Methods

A properly formed \mathbf{S}^{PQ} matrix with $\mathcal{M} > 2\mathcal{L}$ will be full rank, allowing for simultaneous estimation of real and reactive power using voltage data only and the distinct real and reactive power sensitivity signatures. However, there may be multicollinearity between the columns of the interleaved \mathbf{S}^{PQ} . Therefore, the least-squares estimator, while very unbiased, may potentially have high variance [16]. Therefore, the least-squares solution outlined above may not always be an ideal solution in practice. Shrinkage estimators, which reduce the variance in exchange for the introduction of more bias [17], apply well to this problem in the following two scenarios: ① an ill-posed estimation; ② a more realistic large feeder.

There are several instances where an ill-posed estimation could be faced. As the number of candidate injection columns in \mathbf{S}^{PQ} approaches the number of measurement buses, i.e., $2\mathcal{L} \rightarrow \mathcal{M}$, we are exposed to a higher risk of overfitting and multicollinearity in the sensitivities as \mathbf{S}^{PQ} . When $\mathcal{L} >$

$\mathcal{M}/2$, the estimation will become underdetermined.

If the distribution model used to derive the sensitivity matrix is significantly incorrect or out of date, some of the sensitivity signatures may be a poor basis for the model, and there may be instability in the fit against the observed measurement data. In these instances, the high variance of the least-square estimator can be combated by applying ridge regression, which allows the user to place a penalty to the L_2 norm of the solution, thus biasing the model toward the solutions that are more regular. This may significantly improve the predictive accuracy of the model.

Forming an underdetermined sensitivity matrix (more columns than rows) may also be necessary if the distribution engineer has the uncertainty about the DER location, but still wishes to estimate the power factor settings. In this case, a higher-dimensional underdetermined \mathbf{S}^{PQ} will result in few coefficients of the injection estimation vector $\hat{\mathbf{x}}$ being relevant to the estimation of the DER's power factor. This can be cast as a sparse approximation problem. In this case, to form our model, we apply an L_1 norm penalty to the least-squares model that we developed previously and optimize for the weight of the penalty that yields the strongest predictive power. This technique is also known as the least absolute shrinkage and selection operator (LASSO) and has the convenient ability to perform simultaneous model selection and feature extraction [17], yielding a very sparse $\hat{\mathbf{x}}$. This will help address the instability in the estimate as \mathcal{L} approaches $\mathcal{M}/2$. In the case of uncertain DER location, we propose the sparse approximation model (12), which is an augmented form of the problem in (11):

$$\hat{\mathbf{x}}_{lasso} = \underset{\mathbf{x} \in \mathbb{R}^{2\mathcal{L}}}{\operatorname{argmin}} \|\bar{\mathbf{d}} - \mathbf{S}^{PQ} \mathbf{x}\|_2^2 + \lambda \|\mathbf{x}\|_1 \quad (12)$$

where $\lambda > 0$ is the Lagrangian penalty factor set by the user. This method, also known as the basis pursuit, promotes sparsity. This means that the resulting estimation vector $\hat{\mathbf{x}}$ will have a small number of nonzero components. Unlike the least-squares formulation, there is no closed-form solution [17], and it consists of solving the following constrained optimization problem:

$$\begin{cases} \hat{\mathbf{x}}_{lasso} = \underset{\mathbf{x} \in \mathbb{R}^{2\mathcal{L}}}{\operatorname{argmin}} \|\bar{\mathbf{d}} - \mathbf{S}^{PQ} \mathbf{x}\|_2^2 \\ \text{s.t. } \|\mathbf{x}\|_1 \leq \lambda \\ \lambda > 0 \end{cases} \quad (13)$$

The equivalent Lagrangian form can also be expressed as:

$$\hat{\mathbf{x}}_{lasso} = \underset{\mathbf{x} \in \mathbb{R}^{2\mathcal{L}}}{\operatorname{argmin}} \sum_{m=1}^{\mathcal{M}} (\bar{d}_m - \mathbf{s}_m^T \mathbf{x})^2 + \lambda \sum_{l=1}^{2\mathcal{L}} |x_l| \quad (14)$$

where \bar{d}_m is an element of the measurement vector observed; and \mathbf{s}_m^T is a particular row of \mathbf{S}^{PQ} .

For cases where there is a high degree of multicollinearity in the sensitivity matrix, e.g., a poor or inaccurate distribution model, we propose the use of ridge regression [17], and the estimation vector becomes the solution to:

$$\hat{\mathbf{x}}_{ridge} = \underset{\mathbf{x} \in \mathbb{R}^{2\mathcal{L}}}{\operatorname{argmin}} \|\bar{\mathbf{d}} - \mathbf{S}^{PQ} \mathbf{x}\|_2^2 + \lambda \|\mathbf{x}\|_2^2 \quad (15)$$

This can be converted to the standard least-squares solution in (11) by concatenating $\sqrt{\lambda} \mathbf{I}$ to the bottom of \mathbf{S}^{PQ} and zeros to the bottom of $\bar{\mathbf{d}}$, allowing for a closed-form solution.

This technique smooths out singularities in the sensitivity data. Similar to least-squares, it is assumed that the coefficients of $\hat{\mathbf{x}}_{lsq}$ and the residuals of this estimate will also be normally distributed [18].

For both of the regularized regression models described in (12) and (15), the norm penalty λ can easily be chosen in practice using modern cross-validation algorithms such as those in [19].

C. Statistical Analysis

1) Chi-squared Goodness-of-fit

A chi-squared goodness-of-fit test can be used for the least-squares procedure by noting that the estimated voltage magnitude deviations $\hat{\mathbf{d}}$ can be given by $\mathbf{S}^{PQ}\hat{\mathbf{x}}$. By the central limit theorem, the normalized residuals of these voltage deviations are assumed to be distributed according to a standard normal, i.e.,

$$r_i = \frac{\hat{d}_i - \bar{d}_i}{\sigma_i} \sim \mathcal{N}(0, 1) \quad \forall i \in [1, \mathcal{M}] \quad (16)$$

where \hat{d}_i is the element of $\hat{\mathbf{d}}$; and r_i is the residual.

Voltage meters typically have an error of at most less than one percent, so it is assumed that $\sigma_i = (0.01)$, $i = 1, 2, \dots, \mathcal{M}$. Note that this is a worst-case scenario, and most meters in practice have errors of less than half a percent.

The least-squares solution $\hat{\mathbf{x}}_{lsq}$ minimizes the sum of squares of the residuals r_i according to the definitions in (11). Hence, we can compute the chi-squared test statistic as:

$$\|\bar{\mathbf{d}} - \mathbf{S}^{PQ}\hat{\mathbf{x}}\|_2^2 = \chi^2 \geq \zeta \triangleq \|\bar{\mathbf{d}} - \mathbf{S}^{PQ}\hat{\mathbf{x}}\|_2^2 \quad (17)$$

The value of ζ can be written succinctly as:

$$\zeta(\hat{\mathbf{x}}) = (\mathbf{S}^{PQ}\hat{\mathbf{x}} - \bar{\mathbf{d}})^\top \mathbf{\Omega}^{-1} (\mathbf{S}^{PQ}\hat{\mathbf{x}} - \bar{\mathbf{d}}) \quad (18)$$

where $\mathbf{\Omega}^{-1}$ is defined as:

$$\mathbf{\Omega}^{-1} \triangleq \begin{bmatrix} \frac{1}{\sigma_i} & 0 & \dots & 0 \\ 0 & \frac{1}{\sigma_i} & \dots & 0 \\ \vdots & \vdots & \ddots & \vdots \\ 0 & 0 & \dots & \frac{1}{\sigma_i} \end{bmatrix} \quad (19)$$

Using the observations above, we can then perform a chi-squared goodness-of-fit test with $\nu = \mathcal{M} - (2\mathcal{L} + 1)$ degrees of freedom:

$$\mathbb{P}[\chi^2 \geq \zeta] = 1 - \mathbb{P}[\zeta, \nu] \quad (20)$$

where $\mathbb{P}[\chi^2 \geq \zeta]$ is the goodness-of-fit heuristic of the injection estimates used as the basis for the power factor estimation given the sensitivity model.

However, the validity of (17) does not hold for the shrinkage estimates $\hat{\mathbf{x}}_{lasso}$ and $\hat{\mathbf{x}}_{ridge}$, as these estimates by definition do not always reach the global minimum sum of squared errors. Goodness-of-fit tests for LASSO, ridge, and other regularized regression estimates are actually only a recent topic, see [20], and the application of these tests to this problem will be left for future work.

2) Confidence Intervals

Reference [16] also describes a $100 \times (1 - \alpha)\%$ confidence interval for each of the multiple linear regression coefficients \hat{x}_i :

$$\hat{x}_i \pm t_{\alpha/2, \mathcal{M} - (2\mathcal{L} + 1)} \sqrt{K_{ii}} \quad (21)$$

where K_{ii} is the diagonal element of the variance-covariance matrix \mathbf{K} for the estimated regression coefficients, defined as:

$$\mathbf{K} = \hat{\sigma}^2 ((\mathbf{S}^{PQ})^\top \mathbf{S}^{PQ})^{-1} \quad (22)$$

where $\hat{\sigma}^2$ is the mean squared error (MSE) of the model.

Similar to the chi-squared goodness-of-fit test, this analytic confidence interval can only be obtained for the least-squares estimator. However, a well-known method for achieving a confidence interval that is applicable to all of the aforementioned methods, including least-squares, is the bootstrap method [17].

Note that the entries of our parameter estimate $\hat{\mathbf{x}} \triangleq [x_1, x_2, \dots, x_{2\mathcal{L}}]$ are the projections of $\bar{\mathbf{d}}$ onto the subspace \mathbf{S}^{PQ} , as described in (9). This interpretation of the model holds for all estimators developed. To obtain confidence intervals for each injection coefficient, we can draw Q subsets of a random \tilde{N} rows of \mathbf{S}^{PQ} and $\bar{\mathbf{d}}$ entries, yielding augmented regression data denoted as $\tilde{\mathbf{S}}^{PQ}$ and $\tilde{\mathbf{d}}$. At each iteration, we then estimate a new $\tilde{\mathbf{x}}$ from projecting $\tilde{\mathbf{d}}$ onto the \tilde{N} rows of $\tilde{\mathbf{S}}^{PQ}$. This method captures the variance in the estimate attributable to the data [17], [21].

We can obtain a maximum likelihood estimate of the expected value for the injection estimates $\tilde{\mathbf{x}}$ by finding the sample mean of the bootstrapped statistic:

$$\tilde{\mathbf{x}} = \hat{\mathbb{E}}[\hat{\mathbf{x}}] = \frac{\sum_{b=1}^Q \tilde{\mathbf{x}}_b}{Q} \quad (23)$$

For least-squares regression models, it holds that bootstrap confidence intervals are exactly equivalent to the analytic confidence intervals described in (21) as $Q \rightarrow \infty$ [17]. Therefore, we use this method to compare the confidence of each of the proposed estimation methods.

We propose the use of a nonparametric bootstrap confidence interval, specifically the percentile methodology, which is frequently used for the estimators we have selected. Through the resampling process described above, we can obtain an approximate distribution $f(\tilde{x}_i)$ for the \tilde{x}_i coefficient of interest using this method. Finally, a $100 \times (1 - \alpha)\%$ confidence interval for the coefficient can be obtained using the percentiles. In symbols, this would be the $(\tilde{x}_i^{\alpha/2}, \tilde{x}_i^{1-\alpha/2})$ such that:

$$\left(\int_{-\infty}^{\tilde{x}_i^{\alpha/2}} f(\tilde{x}_i) d\tilde{x}_i, \int_{-\infty}^{\tilde{x}_i^{1-\alpha/2}} f(\tilde{x}_i) d\tilde{x}_i \right) = \left(\frac{\alpha}{2}, 1 - \frac{\alpha}{2} \right) \quad (24)$$

IV. ALGORITHM IMPLEMENTATION

The sensitivity matrix can be understood as a static, model-based quantity fixed intertemporally for the power system under analysis. The construction of this matrix is straightforward and is outlined in Algorithm 1.

Algorithm 1: sensitivity matrix construction

Result: returns the S^{PQ} matrix for the model

Initialization

Lock voltage regulating devices

Solve base case powerflow

Retrieve $V_{base}=(v_i), \forall i \in \mathcal{M}$

Define counter $k=0$

for $l \in \mathcal{L}$ **do**

if $mod(k,2) \neq 0$ **then**

 Place reactive power injection

 Solve power flow

 Retrieve $V=(v_i), \forall i \in \mathcal{M}$

$S_l^{PQ}=V-V_{base}$

else

 Place real power injection

 Solve power flow

 Retrieve $V=(v_i), \forall i \in \mathcal{M}$

$S_l^{PQ}=V-V_{base}$

end

$k=k+1$

end

Figure 3 shows the visualization of sensitivity columns in S^{PQ} formed with 100 kW or 100 kvar injections on IEEE 13-bus test feeder.

As discussed previously, S^{PQ} must be full rank to perform the estimation. Depending on the power system modeled, some columns may have linear dependencies, because the nodes that they represent may be electrically identical. For instance, the IEEE 13-bus test feeder has a switch between buses 671 and 692 [22], [23], which is closed by default. Thus, when constructing S^{PQ} with static injections as in Algorithm 1, the columns associated with real and reactive power

injections for these two buses will be linearly dependent and S^{PQ} will become rank-deficient. A simple solution is to use a distance metric e.g., the L_1 norm of the residuals between each column as shown in (25), as a method for measuring the similarity between S^{PQ} columns s_{l_1} and $s_{l_2} \forall l_1, l_2 \in \mathcal{L}$. The user can then discard the rows and columns corresponding to one of the indices from each pairwise comparison to solve the rank deficiency.

$$d_{L_1}(s_{l_1}, s_{l_2}) = \|s_{l_1} - s_{l_2}\|_1 = \sum_{m=1}^M |s_{l_1,m} - s_{l_2,m}| \quad (25)$$

For the IEEE 13-bus test feeder, we discard the rows and columns associated with bus 692, yielding a full rank matrix. We also use the similarity metric (25) for a hierarchical clustering of the sensitivities, using the single linkage clustering algorithm described in [24].

The visualization of sensitivity columns in an example S^{PQ} matrix formed with 100 kW or 100 kvar injections on the IEEE 13-bus test feeder is shown in Fig. 3. The columns are clustered according to their L_1 distances, as described in (25). The columns corresponding to real and reactive power sensitivities are labeled as green and purple, respectively. The numbers of clusters are increased iteratively until they are equal to the $2\mathcal{L}$ injection candidates. If six clusters are chosen, the clusters correspond to common injection type and injection phase. This further verifies the result that the voltage magnitude sensitivity signatures are distinct.

Using the injection estimation methods, we form Algorithm 2 to estimate the power factor of the nodes $\mathcal{L} \subset \mathcal{M}$ of interest. Many real-world inverter systems are three-phase. Thus, generality for three-phase estimations is included. With any of the estimation methods described in the paper, the basic relationships between the complex apparent power and power factor are used to form an estimate for the power factor from the estimated injections.

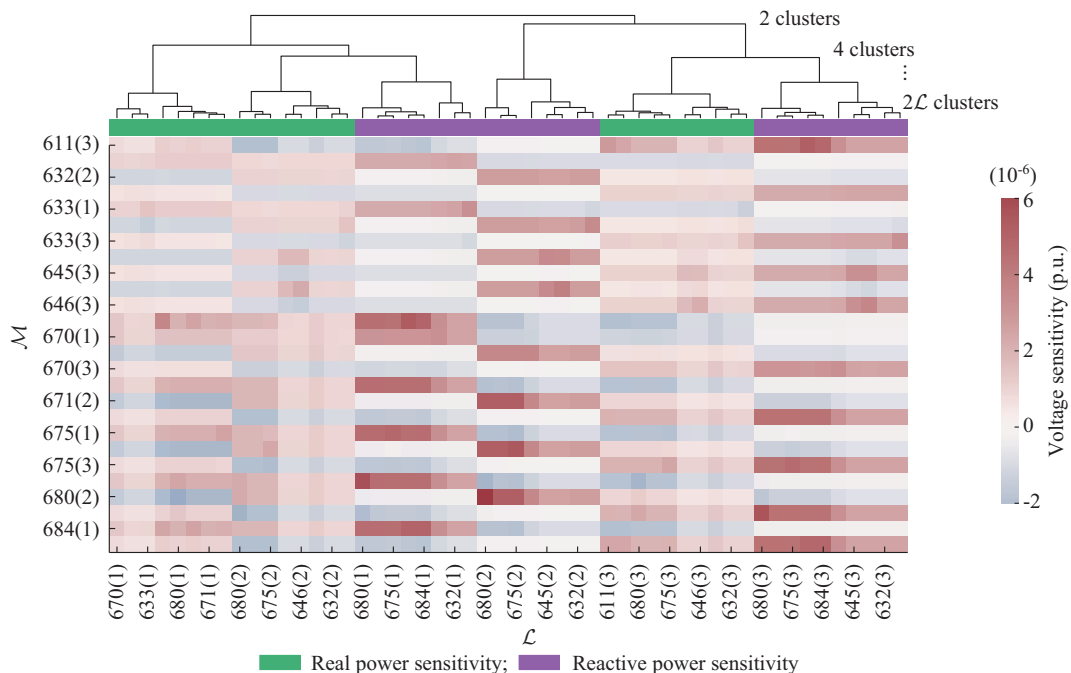


Fig. 3. Visualization of sensitivity columns in S^{PQ} formed with 100 kW or 100 kvar injections on IEEE 13-bus test feeder.

Algorithm 2: power factor estimation procedure

Result: returns an estimation of the power factor of DER systems operating on nodes $\mathcal{L} \subset \mathcal{M}$

Initialization

Load network model

Retrieve $V_{base} = (v_i), \forall i \in \mathcal{M}$

Compute S^{PQ} (Algorithm 1)

Define injection buses $\mathcal{L} \subset \mathcal{M}$

Load historical voltage measurements

Retrieve $V = (v_i), \forall i \in \mathcal{M}$

Compute \hat{d} ((7) and (8))

Compute \hat{x} ((11), (12), or (15))

Define $P, Q \in \mathbb{R}^{1 \times 2\mathcal{L}}$

if system is three phase **then**

for each \hat{x}_p , each phase **do**

if injection type is real **then**

$P_i = \hat{x}_i$

else

$Q_i = \hat{x}_i$

end

end

else

for each \hat{x}_i **do**

if injection type is real **then**

$P_i = \hat{x}_i$

else

$Q_i = \hat{x}_i$

end

end

end

for each $P_i, Q_i \in [P, Q]$ **do**

$S_i = \sqrt{P_i^2 + Q_i^2}$

$\hat{pf}_i = \frac{|P_i|}{S_i}$

end

V. CASE STUDIES AND NUMERICAL RESULTS

In this section, we present the results for two case studies using a small (IEEE 13-bus) feeder and a larger (IEEE 123-bus) feeder to demonstrate the performance of the algorithms. The sensitivity matrix models for the feeders are constructed according to (1) and Algorithm 1. As described previously, identical points are identified and filtered using (25), with an L_1 tolerance of 1×10^{-12} , and the removal decisions are verified by referencing [23], [25]. We then estimate the power factor control settings using the process described in Algorithm 2.

Typically, a DER system outputs a mixture of real and reactive power at the interconnection point. Thus, we will show the results obtained when static injections of real and reactive power are placed on the buses of interest. This model represents a particular measurement instance where a grid-connected PV system simultaneously generates real power, and the PCC voltage is being regulated by a reactive power injection or absorption by its advanced inverter system.

A. Small Feeder and Ridge

For this experiment, we consider two static three-phase injections on buses 633 and 671 of the IEEE 13-bus feeder, as shown in Fig. 4.

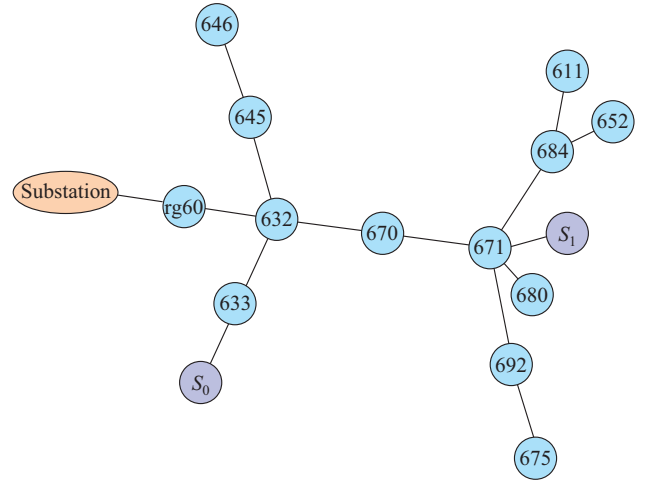


Fig. 4. Graph plot of IEEE 13-bus feeder showing interconnection locations for static systems.

By using Algorithm 1, the sensitivity matrix is constructed and preprocessed as described previously using (25). Using the first control flow of Algorithm 2, the estimation vector \hat{x} can be formed, and the estimated injection states derived from the \hat{x} coefficients can easily be used to compute an estimate for the power factor of the PV systems according to the third control flow of Algorithm 2.

When the estimation problem is well posed, i.e., $M \gg \mathcal{L}$, least-squares regression can be used without issue, yielding accurate estimates for the injections and power factor shown in Figs. 5 and 6. In Fig. 5, \hat{P}_1 and \hat{Q}_1 are the entries of \hat{x} that corresponding to real and reactive power injections, respectively. The inherent difference in the voltage sensitivity signatures is realized, and accurate numerical results and mean errors from the theoretical values are shown in Table I. χ^2 goodness-of-fit statistics also show favorable results for the accuracy, as shown in Table II.

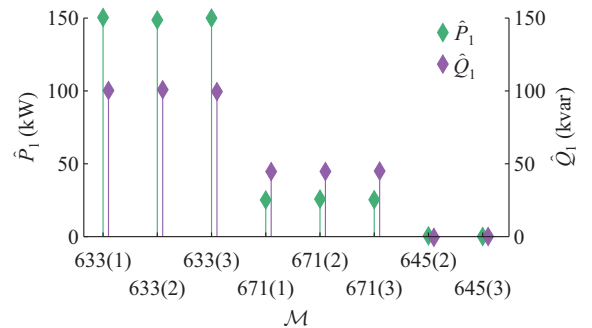


Fig. 5. Well-posed ($M=26 > 2\mathcal{L}=16$) least-squares injection estimate for three-phase injections.

The least-squares injection estimate is highly unbiased, as is the case with all least-squares estimators. However, these estimators typically have a high variance.

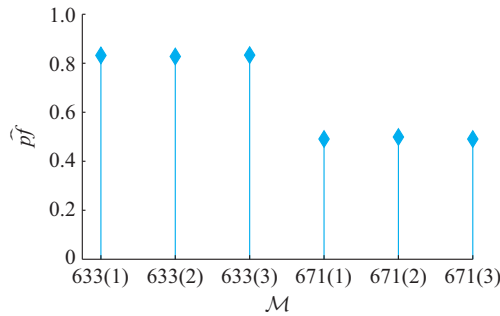


Fig. 6. Well-posed least-squares power factor estimation for three-phase injections.

TABLE I
WELL-POSED LEAST-SQUARES ESTIMATION RESULTS

Scenario	Node (phase)	Injection (kVA)	Power factor
Actual	633(1)	150+j100	0.83205
	633(2)	150+j100	0.83205
	633(3)	150+j100	0.83205
	671(1)	25+j45	0.48564
	671(2)	25+j45	0.48564
	671(3)	25+j45	0.48564
Estimated	633(1)	150.66+j100.43	0.83207
	633(2)	148.24+j101.07	0.82621
	633(3)	150.36+j99.15	0.83484
	671(1)	25.15+j44.57	0.49137
	671(2)	25.95+j44.66	0.50234
	671(3)	25.38+j45.10	0.49082
Mean error (%)		0.0156	0.8870

TABLE II
 χ^2 GOODNESS-OF-FIT STATISTICS FOR IEEE 13-BUS LEAST-SQUARES ESTIMATES

PCC	ξ	$\mathbb{P}[\chi^2 \geq \xi]$
633	2.57×10^{-22}	0.9999
671	3.71×10^{-21}	0.9999
670	5.69×10^{-18}	0.9999
632	3.56×10^{-19}	0.9999

To illustrate this tradeoff, Fig. 7 shows bootstrap sampling distributions for a subset of least-squares injection estimate coefficients of the IEEE 13-bus model: \hat{x}_0 (633(1), real power), \hat{x}_1 (633(1), reactive power), \hat{x}_6 (671(1), real power), and \hat{x}_7 (671(1), reactive power). In Fig. 7, $\hat{f}(\hat{x})$ is the sample frequency. Dashed lines indicate the means of the distributions, which are equivalent to the estimates in Fig. 4. High accuracy is observed, but the estimator has high variance.

With least-squares, while the mean of the coefficient distribution in principle represents a highly accurate estimate of the true parameter, the precision, clearly, may be low for small feeders. This is because for small feeder models such as the IEEE 13-bus case, the \mathcal{S}^{pq} matrix has limited samples ($\mathcal{M}=26$), which can be attributed to the variance in the coefficient distribution.

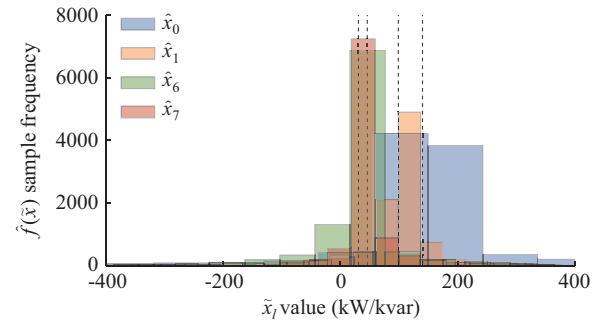


Fig. 7. Bootstrap sampling distributions for a subset of least-squares injection estimate coefficients of IEEE 13-bus model.

As we expand the number of candidate injections in \mathcal{S}^{pq} , the problem becomes ill-posed, and the risk of overfitting to the sensitivities increases dramatically. In our experiments, a large amount of instability in the least-squares solution \hat{x}_{lsq} is observed when candidate injection columns $2\mathcal{L}=25$ are used in \mathcal{S}^{pq} . However, using the shrinkage estimator \hat{x}_{ridge} , a much more accurate solution is obtained.

Figure 8 shows the ill-posed ridge regression estimation vector for three-phase injections. If we use least-squares, the estimate would be highly unstable, and we would effectively fit to the noise of the sensitivity data because \mathcal{M} is close to $2\mathcal{L}$. By applying ridge regression, we can consider more candidate buses in exchange for more bias in the estimate.

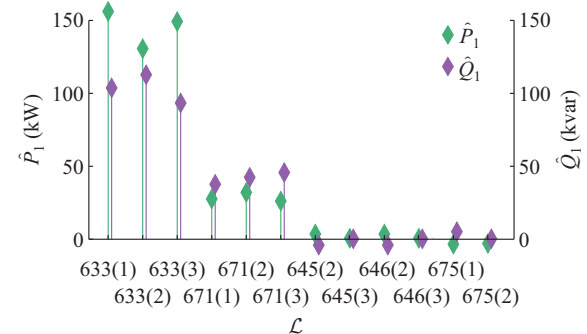


Fig. 8. Ill-posed ridge regression injection estimation vector for three-phase injections.

B. Large Feeder and LASSO

Distribution engineers may be interested in a wider range of candidate buses when considering feeder models such as the IEEE 123-bus case. Furthermore, in large feeder models, it may be more difficult to preprocess the \mathcal{S}^{pq} matrix so that electrically identical rows and columns are removed due to incomplete information regarding the state of the switches. Figure 9 shows the results of LASSO estimation methods outlined in (12). In this experiment, a 10-fold cross-validation is used to select the Lagrange multiplier λ .

Figure 9 demonstrates the simultaneous feature selection and model fitting capabilities of the method. The LASSO estimate is biased toward sparse estimates in favor of lowering the variance of the estimator. Since this example exhibits single-phase injections, this model is ideal. LASSO is useful when the distribution engineer knows with high confidence

that there are few distributed generators on the candidate buses measured, meaning that few corresponding columns of \mathbf{S}^{PQ} are relevant. The penalty on the L_1 norm of $\hat{\mathbf{x}}$ favors sparsity for the solution and improves the interpretability of the model in these application scenarios.

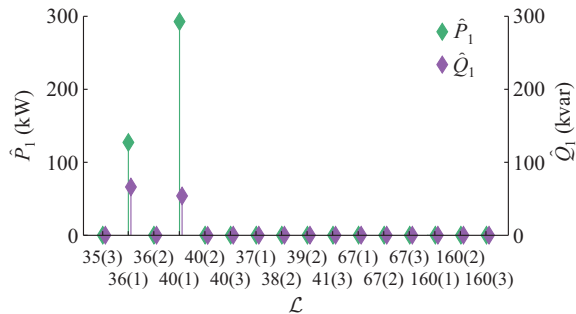


Fig. 9. LASSO regression coefficients for single-phase injections.

Like ridge, LASSO coefficients also exhibit significantly less variance, as shown in Fig. 10 and Table III. When using regularized estimates in the right context, significantly better precision and interpretability of the power factor estimation can be achieved.

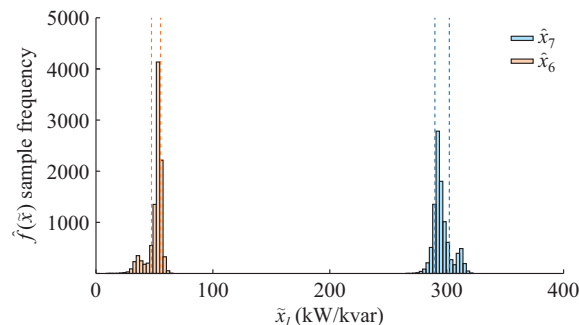


Fig. 10. Example of bootstrap sampling distributions for a subset of LASSO injection estimate coefficients for IEEE 123-bus model.

TABLE III
CONFIDENCE INTERVALS FOR IEEE 123-BUS LASSO ESTIMATES

α	\hat{x}_7		\hat{x}_6	
	$\tilde{x}_{\alpha/2}$	$\tilde{x}_{1-\alpha/2}$	$\tilde{x}_{\alpha/2}$	$\tilde{x}_{1-\alpha/2}$
0.050 (95%)	32.819	57.919	283.908	314.041
0.320 (68%)	47.262	55.264	289.787	302.131

Further details of the behavior of the optimization algorithm are shown in Fig. 11, showing the effect of the Lagrangian penalty factor λ on the model coefficients and the MSE with each fold of the cross-validation procedure, where a new λ value is selected.

In Fig. 11, we also show one solution for selecting the hyperparameters of the regularized estimators. Figure 11(a) shows the values of the parameters in the estimation vector $\hat{\mathbf{x}}_{lasso}$, and Fig. 11(b) shows the MSE of the estimate, both as functions of the negative natural logarithm of the penalty factor λ .

To generate the trace in Fig. 11(a), we used 10-fold grid-search CV [17], [19], which iteratively splits the rows of \mathbf{S}^{PQ}

into nine test groups and seeks to find the value of λ that generates the lowest MSE values for predicting the remaining fold. The range of $-\log(\lambda)$ values considered is shown on the x-axis. In Fig. 11(b), we show the MSE at each fold. The final value of $-\log(\lambda)$ is indicated by the dashed vertical line.

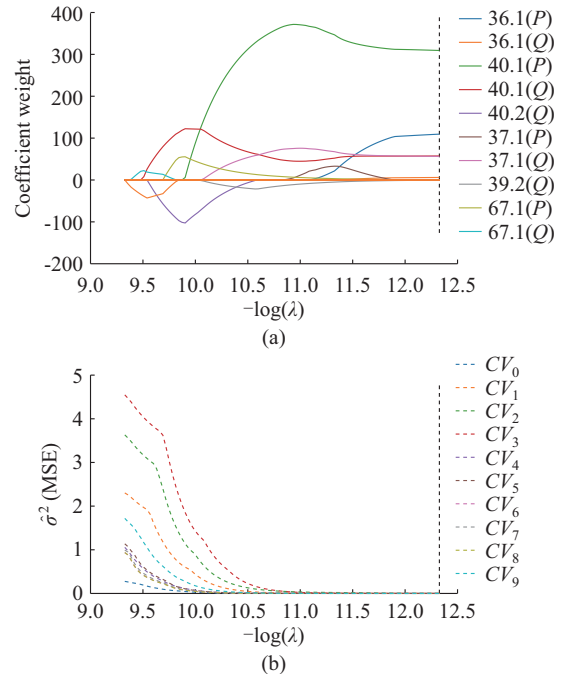


Fig. 11. LASSO injection estimate coefficients and MSE trace plots versus $-\log(\lambda)$. (a) Coefficients weights versus $-\log(\lambda)$. (b) MSE versus $-\log(\lambda)$.

VI. DISCUSSION

There are several key limitations to the results in this paper. The preprocessing of time-series data in forming the $\bar{\mathbf{d}}$ vector has not yet been fully solved. If the user only has access to this type of data, determining which subset of \mathbf{D}' to sample as $\bar{\mathbf{d}}$ may be challenging. Figure 2 illustrates this challenge by showing the values of \mathbf{D}' as defined in (5), for all values of $i \in \mathcal{M}$ and $t \in T$ for an injection scenario with power factor of 0.8.

A practical solution is to select a window of $\bar{\mathbf{d}}$ values in the midday period of the time-series. Recent developments in the field of statistical learning could be used to perform feature extraction or selection to identify the timepoints of interest [26], [27]. In time-series modeling, the estimation becomes less accurate when there is less difference in the voltage from power injections during nighttime and cloudy days.

As for many physics-based inverse problems, the estimation methods provided in this paper may have a high degree of variance. Additional improvements could be studied to determine the proper amount of bias to add to the estimators to enable more interpretable models, particularly when working with non-midday time-series data.

An additional limitation of these methods is that the rough location of the distributed generator is assumed to be known. However, [13], [14], [28] could be used in tandem with this method to first estimate the location of an un-

known distributed generator, and then the algorithms proposed in this paper could be applied to a constrained set of candidate injection locations to estimate the power factor of the DER. Another potential solution to this problem would be statistical methods such as best subset selection [17] or other regularization methods such as the LASSO method presented in this paper. If the user does not have confidence that the selected candidate injection locations contain a generator, it cannot be guaranteed that the observed voltage magnitude deviations in the data will be attributable to a distributed generator. In these instances, the estimation may be less interpretable.

Future works will include a more robust time-series feature extraction method as well as the extension of these methods to the estimation of other inverter parameters such as control settings and curtailment.

VII. CONCLUSION

This research has presented a novel physics-based and data-driven method to estimate the injection state and power factor of inverter-based DERs. Based purely on voltage magnitude measurements and model-derived sensitivities, flexible estimation approaches have been developed for various realistic use cases.

Firstly, we have shown that for a fixed power system model with a properly constructed \mathcal{S}^{PQ} sensitivity matrix, the real and reactive power voltage sensitivity signatures for a set of candidate buses under study are linearly independent, in which case, \mathcal{S}^{PQ} is full rank. Notably, we have also shown that there exists a significant enough difference between these signatures to estimate the real and reactive power injection states of inverter-based DERs using purely voltage measurements and linear parameter estimation models.

Additionally, we have shown that regularization methods are highly effective at improving the precision of the linear models in certain use case scenarios. Often, the least squares model may not be a viable option from a practical standpoint. For models with poor goodness of fit as derived in Section II, or when the model characteristics meet those described in Section III, the regularized methods will often be necessary, and will improve the estimation performance.

As the demand and need for solar PV and other inverter-based DERs increase, it is vital to access the information that characterizes these oftentimes unobservable distributed systems for ensuring a smooth transition to a decarbonized grid. These algorithms can be used in power system planning, operation, and control applications to give utilities and ISOs with the ability to estimate important control parameters and the operating point of these distributed generation systems. This can be of service in bolstering sustainable power system planning and decarbonization efforts.

REFERENCES

- [1] M. U. Qureshi, S. Grijalva, and M. J. Reno, "A fast quasi-static time series simulation method for PV smart inverters with VAR control using linear sensitivity model," in *Proceedings of 2018 IEEE 7th World Conference on Photovoltaic Energy Conversion (WCPEC)*, Waikoloa, USA, Jun. 2018, pp. 1614-1619.
- [2] S. Deshmukh, B. Natarajan, and A. Pahwa, "State estimation and voltage/var control in distribution network with intermittent measurements," *IEEE Transactions on Smart Grid*, vol. 5, no. 1, pp. 200-209, Jan. 2014.
- [3] Q. Long, J. Wang, D. Lubkeman *et al.*, "Volt-var optimization of distribution systems for coordinating utility voltage control with smart inverters," in *Proceedings of 2019 IEEE PES Innovative Smart Grid Technologies Conference (ISGT)*, Washington, USA, Feb. 2019, pp. 1-5.
- [4] A. O'Connell and A. Keane, "Volt-var curves for photovoltaic inverters in distribution systems," *IET Generation, Transmission & Distribution*, vol. 11, no. 3, pp. 730-739, Mar. 2017.
- [5] *IEEE Standard for Interconnection and Interoperability of Distributed Energy Resources with Associated Electric Power Systems Interfaces*, IEEE Standard 1547-2018, 2018.
- [6] L. Blakely, M. J. Reno, and J. Peppanen, "Identifying common errors in distribution system models," in *Proceedings of 2019 IEEE 46th Photovoltaic Specialists Conference (PVSC)*, Chicago, USA, Jun. 2019, pp. 3132-3139.
- [7] K. Christakou, J. LeBoudec, M. Paolone *et al.*, "Efficient computation of sensitivity coefficients of node voltages and line currents in unbalanced radial electrical distribution networks," *IEEE Transactions on Smart Grid*, vol. 4, no. 2, pp. 741-750, Jun. 2013.
- [8] C. McEntee, N. Lu, and D. Lubkeman. (2020, Oct.). A regression-based voltage estimation method for distribution volt-var control with limited data. [Online]. Available: <https://arxiv.org/abs/2010.12456>
- [9] M. Rylander, M. J. Reno, J. E. Quiroz *et al.*, "Methods to determine recommended feeder-wide advanced inverter settings for improving distribution system performance," in *Proceedings of 2016 IEEE 43rd Photovoltaic Specialists Conference (PVSC)*, Portland, USA, Jun. 2016, pp. 1393-1398.
- [10] M. Rylander, J. Smith, and H. Li, "Determination of smart inverter control settings to improve distribution system performance," in *Proceedings of CIGRE US National Committee 2014 Grid of the Future Symposium*, Houston, USA, Oct. 2014, pp. 1-6.
- [11] R. Dobbe, P. Hidalgo-Gonzalez, S. Karagiannopoulos *et al.*, "Learning to control in power systems: design and analysis guidelines for concrete safety problems," *Electric Power Systems Research*, vol. 189, p. 106615, Dec. 2020.
- [12] M. Emmanuel, J. I. G. Miner, P. Gotseff *et al.*, "Estimation of solar photovoltaic energy curtailment due to volt-watt control," *IET Renewable Power Generation*, vol. 14, no. 4, p. 6, Jan. 2020.
- [13] S. Grijalva, A. Khan, J. S. Mbeleg *et al.*, "Estimation of PV location in distribution systems based on voltage sensitivities," in *Proceedings of IEEE North American Power Symposium (NAPS)*, Tempe, USA, Apr. 2021, p. 5.
- [14] C. Gomez-Peces, S. Grijalva, M. J. Reno *et al.*, "Estimation of PV location based on voltage sensitivities in distribution systems with discrete voltage regulation equipment," in *Proceedings of IEEE PowerTech Madrid*, Madrid, Spain, Jun. 2021, pp. 1-6.
- [15] A. Dubey and S. Santoso, "On estimation and sensitivity analysis of distribution circuit's photovoltaic hosting capacity," *IEEE Transactions on Power Systems*, vol. 32, no. 4, pp. 2779-2789, Jul. 2017.
- [16] J. L. Devore and K. N. Berk, *Modern Mathematical Statistics with Applications*, New York: Springer, 2nd ed., 2012.
- [17] T. Hastie, R. Tibshirani, and J. Friedman, *The Elements of Statistical Learning: Data Mining, Inference, and Prediction*, New York: Springer, Jan. 2017.
- [18] W. N. van Wieringen. (2020, Aug.). Lecture notes on ridge regression. [Online]. Available: <https://arxiv.org/abs/1509.09169>
- [19] F. Pedregosa, G. Varoquaux, A. Gramfort *et al.*, "Scikit-learn: machine learning in Python," *Journal of Machine Learning Research*, vol. 12, pp. 2825-2830, Dec. 2011.
- [20] R. Lockhart, J. Taylor, R. J. Tibshirani *et al.*, "A significance test for the lasso," *The Annals of Statistics*, vol. 42, no. 2, pp. 413-468, Apr. 2014.
- [21] A. Davison and D. Hinkley, "Bootstrap methods and their application," *Journal of the American Statistical Association*, vol. 94, p. 5, Jan. 1997.
- [22] W. H. Kersting and G. Shirek, "Short circuit analysis of IEEE test feeders," in *Proceedings of 2012 IEEE PES Transmission and Distribution Conference and Exposition*, New Orleans, USA, May 2012, pp. 1-9.
- [23] W. H. Kersting, *Distribution System Modeling and Analysis*, Boca Raton: CRC Press, 2018.
- [24] D. Müllner. (2011, Sept.). Modern hierarchical, agglomerative clustering algorithms. [Online]. Available: <https://arxiv.org/abs/1109.2378>
- [25] W. H. Kersting, "Radial distribution test feeders," *IEEE Transactions*

on *Power Systems*, vol. 6, no. 3, pp. 975-985, Aug. 1991.

- [26] Y. Sun, J. Li, J. Liu *et al.*, "Using causal discovery for feature selection in multivariate numerical time series," *Machine Learning*, vol. 101, pp. 377-395, Oct. 2015.
- [27] J. Taylor and R. J. Tibshirani, "Statistical learning and selective inference," *Proceedings of the National Academy of Sciences*, vol. 112, pp. 7629-7634, Jun. 2015.
- [28] K. Mason, M. J. Reno, L. Blakely *et al.*, "A deep neural network approach for behind-the-meter residential PV size, tilt and azimuth estimation," *Solar Energy*, vol. 196, pp. 260-269, Jan. 2020.

Samuel Talkington received the B.S. degree in electrical engineering from West Virginia University, Morgantown, USA, in 2020 and is currently working towards the Ph.D. degree in Electrical and Computer Engineering at Georgia Institute of Technology, Atlanta, USA. Prior to Georgia Tech, he completed internships at Mitsubishi Electric Power Products, Inc., Pittsburgh, USA, and the NASA Katherine Johnson Facility, Fairmont, USA. His research interests include decentralized power system control, detection and estimation, mathematical optimization, and economics.

Santiago Grijalva received the Ph.D. degree in Electrical and Computer Engineering from the University of Illinois at Urbana-Champaign, Champaign, USA. He is the Southern Company Distinguished Professor of Electrical and Computer Engineering and Director of the Advanced Computational Electricity Systems (ACES) Laboratory at Georgia Institute of Technology, Atlanta, USA. From 2002 to 2009, he was with PowerWorld Corporation, Champaign, USA. From 2013 to 2014, he was with the National Renewable Energy Laboratory (NREL), Golden, USA as the Founding Director of the Power System Engineering Center (PSEC). He was a Member of the NIST Federal Smart Grid Advisory Committee. His research interests include decentralized power system control, cyber-physical security, and economics.

Matthew J. Reno received the Ph.D. degree in electrical engineering from Georgia Institute of Technology, Atlanta, USA. He is a Principal Member of Technical Staff in the Electric Power Systems Research Department at Sandia National Laboratories, Albuquerque, USA. He leads several projects that are applying cutting edge machine learning algorithms to power system problems. His research interests include distribution system modeling and analysis with big data and high penetrations of PV.